Supplementary Material

Influence of ground-state structure and Mg^{2+} binding on folding kinetics of the guanine-sensing riboswitch aptamer domain

Janina Buck[1,#], Anna Wacker[1,#], Eberhart Warkentin[3], , Jens Wöhnert[2,*], Julia Wirmer-Bartoschek[1]Harald Schwalbe[1,*]

[1]Institute for Organic Chemistry and Chemical Biology, [2]Institute for Molecular Biosciences, Center for Biomolecular Magnetic Resonance, Johann Wolfgang Goethe-University, Max-von-Laue-Strasse 7 & 9, 60438 Frankfurt am Main (Germany). [3]Max-Planck-Institute for Biophysics, Max-von-Laue-Strasse 1, 60438 Frankfurt am Main (Germany)

[#]These authors contributed equally to the work

To whom correspondence should be addressed:
Harald Schwalbe, E-mail: schwalbe@nmr.uni-frankfurt.de
Jens Wöhnert, E-mail : woehnert@bio.uni-frankfurt.de

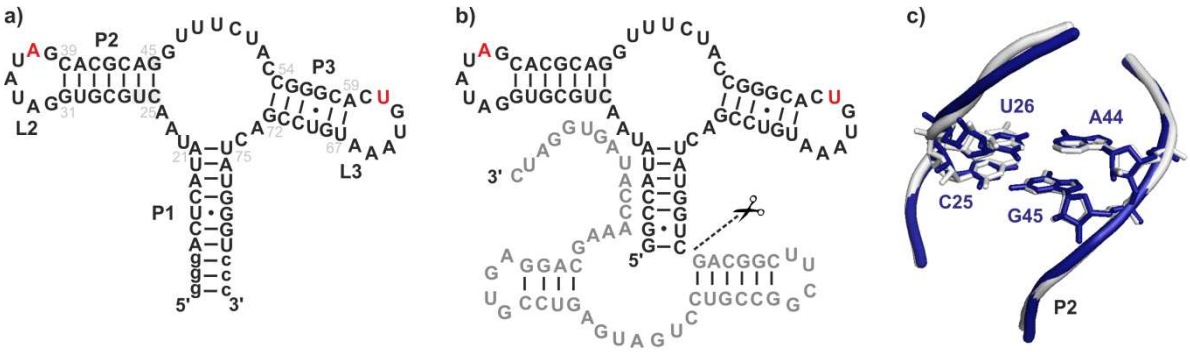

Figure S1: Secondary structures of the G37A/C61U-mutant of the guanine-sensing riboswitch aptamer domain of the *B.subtilis xpt-pbuX* operon (mutated residues at sequence position 37 and 61 are color coded in red); **a)** Gsw^{loop}, including additional nucleotides in helix P1 to allow efficient transcription (lower case letters); **b)** Gsw^{loop}(hh), G37A/C61U-mutant 3'-*hammerhead* construct designed for homogenous 3'-ends for crystallization purposes; Mutations in helix P2 compared to the *wt*-sequence (1) are highlighted in gray on the secondary structures (see Figure S1c); **c)** Close-up view of crystal structure overlay of G37A/C61U-mutant RNA (blue) with the guanine-sensing riboswitch aptamer domain RNA-ligand complex (gray, pdb: 1U8D (2)) shows an identical overall fold with an r.m.s. deviation of ~0.61Å concerning the mutation including sequence context (phosphate backbone of residues 24-27 and 43-46, P2).

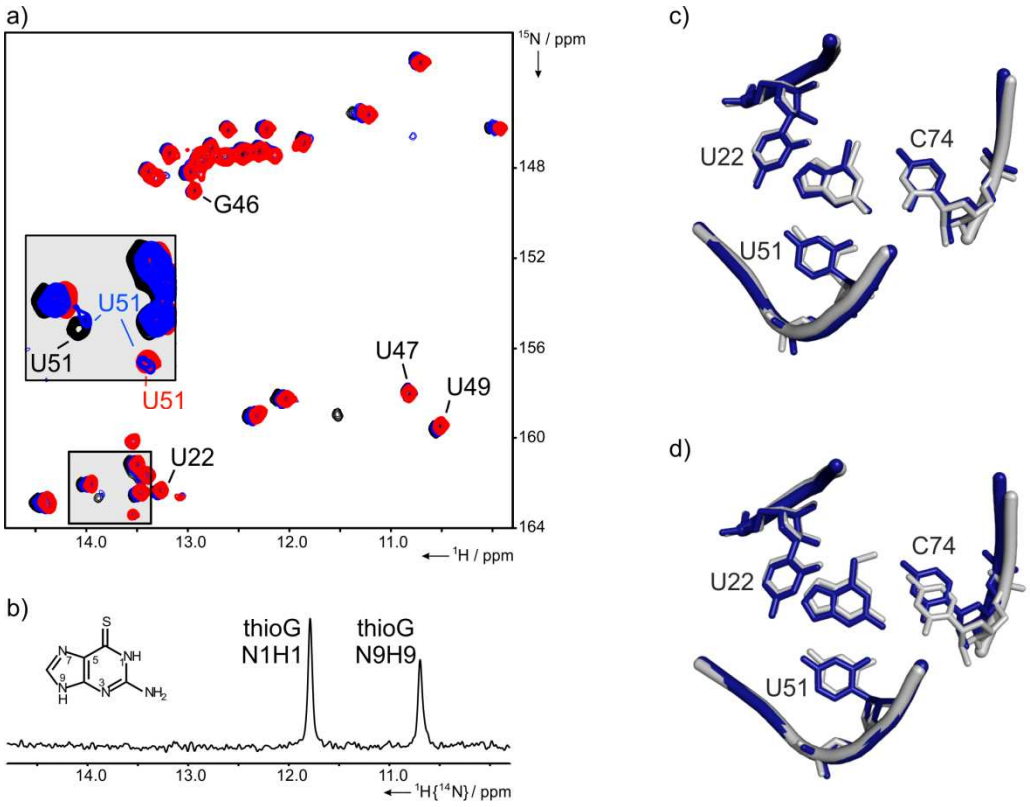

Figure S2: Structural characterization of Gsw^{loop}-thioguanine complex; **a)** temperature-dependent ^{1}H,^{15}N-HSQC spectra, black: 273K, blue: 283K, red: 293K with spectral region of residue U51 enlarged (^{15}N-labeled RNA, unlabeled ligand, 20eq Mg^{2+}). Imino proton resonances of ligand-binding region are annotated; **b)** ^{14}N-edited 1D-^{1}H{^{14}N} imino proton spectrum of Gsw^{loop}-thioguanine complex (^{15}N-labeled RNA, unlabeled ligand, 20eq Mg^{2+}, 293K); NMR imino proton resonances (N1-H1 and N9-H9) of the complexed ligand thioguanine are annotated; **c)** comparison of Gsw^{loop}-thioguanine complex X-ray structure (chain a, blue) with 6-chloro-guanine complex (gray,(3)); **d)** comparison of Gsw^{loop}-thioguanine complex X-ray structure (chain a, blue) with 6-OMe-guanine complex (gray (3)). The binding pocket organization provides an example for structural flexibility of C74 in response to alterations of functional groups, here at the 6-position of the ligand guanine**.**

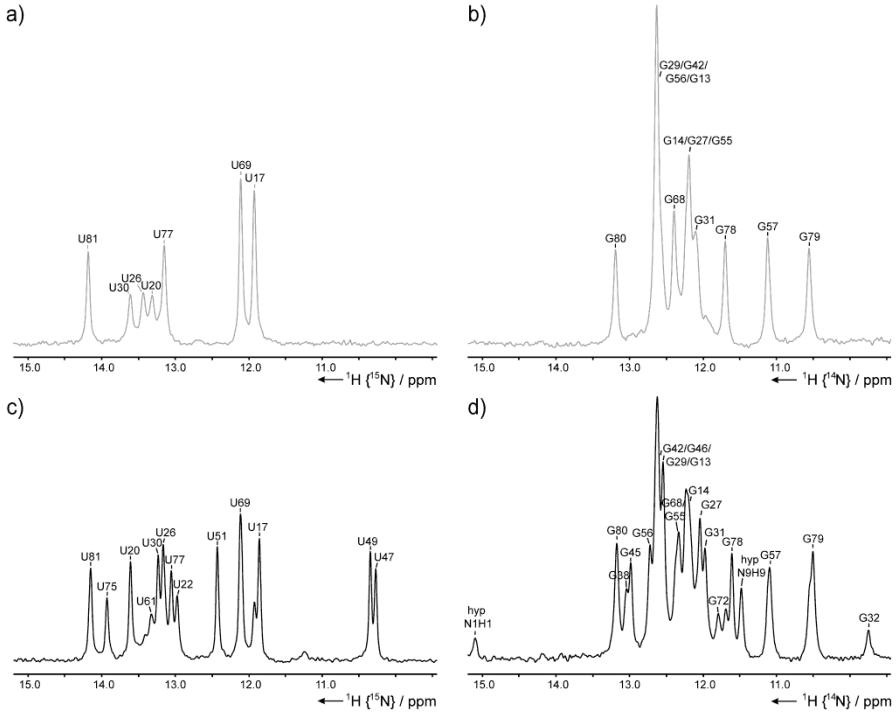

Figure S3: NMR spectra of RNA uridine (*left*, ^{15}N-edited) and guanosine (*right*, ^{14}N-edited) imino proton resonances of the selectively ^{15}N-uridine labeled G37A/C61U-mutant (Gsw^{loop}) with annotated resonance assignment (4) (700MHz, 283K, [RNA]:[Mg^{2+}]-ratio ~1:8). **a)** and **b)** NMR spectra of free RNA before ligand injection; **c)** and **d)** NMR spectra of the Gsw^{loop}-hypoxanthine complex following ligand-induced RNA folding.

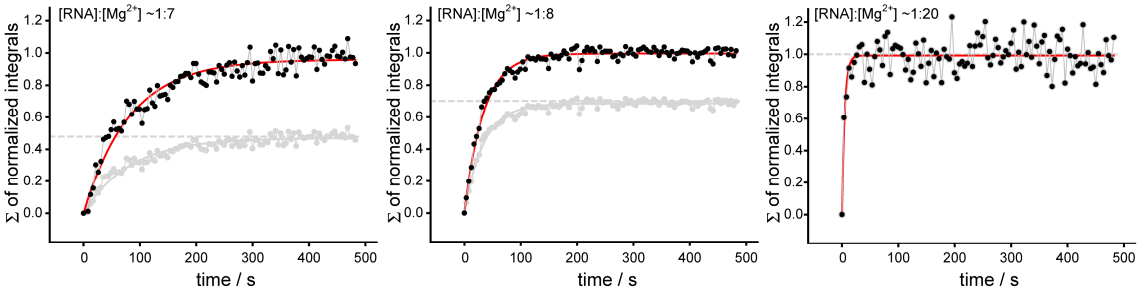

Figure S4: Build-up kinetics for RNA folding at [RNA]:[Mg^{2+}]-ratios of ~1:7, ~1:8 and ~1:20 following ligand injection (signal-to-noise ratio varies depending on the absolute RNA concentration $[RNA]_{abs}$~300-500µM; [RNA]:[hypoxanthine]~1:1). Depicted is the sum of normalized integrals of individual signals (black) at each [RNA]:[Mg^{2+}]-ratio that can be fitted to a monoexponential function (red). Additionally, according to Mg^{2+}-dependent final populations of ligand-bound RNA conformation (Figure 4), the build-up kinetics were normalized (gray).

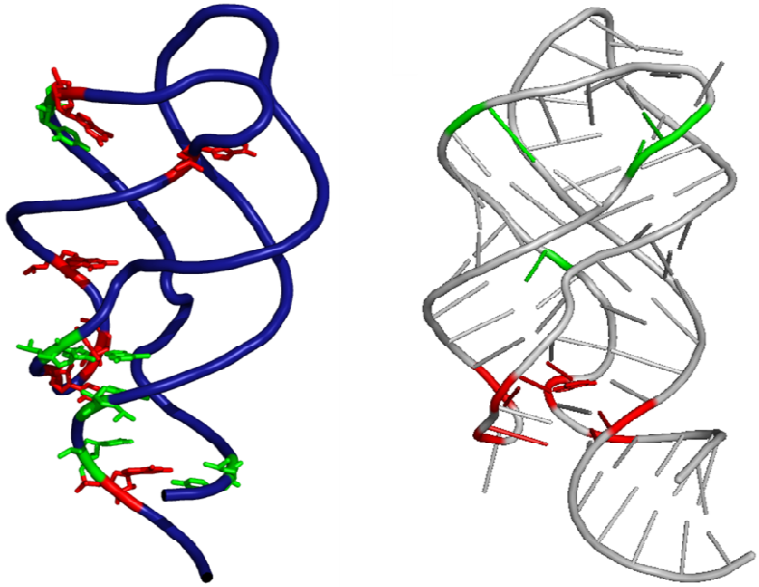

Figure S5: Comparison of the correlation between individual folding rates and sequence position in context of the 3D structure of ligand-bound riboswitch RNAs (wild type Gsw^{apt} (1U8D (2)) and loop mutant Gsw^{loop} (3RKF). We utilize a two color code for $t_{1/2}$ values obtained for the mutant Gsw^{loop} (21±1s (red) and 24±1s (green)) on the crystal structure of the mutant (*left*). Distribution of folding kinetics for the wild type Gsw^{apt} (5) (*right*).

Data collection statistics	
space group	$P3_2$
cell dimension	52.300 52.300 263.400 , 90.00 90.00 120.00
wavelength	1.02
resolution (Å)	44.64-2.50 (2.62 - 2.50)
observed reflections	66897
unique reflections	25949
completeness (%)	93.1 (80.6)
I/s	16.4 (1.7)
R_{merge}	9.2
twin law	-h,-k, l
twin fraction	0.466
Refinement statistics	
resolution (Å)	44.64-2.50 (2.62 - 2.50)
reflections working set	24560
reflections test set	1156
R_{work}	20.7
R_{free}	22.6
RMSD bonds	0.002
RMSD angles	0.492
average B-factor	53.7
cross-val. luzzati coordinate error	0.41
cross-val. sigma-a coordinate error	0.82
pdb-code	3RKF

Table S1: X-ray data collection and refinement statistics.

residue	**k** [s^{-1}]	$t_{1/2}$ [s]
U17	0.029 ± 0.002	24.0 ± 1.4
U30	0.028 ± 0.002	24.5 ± 1.5
G31	0.031 ± 0.002	22.7 ± 1.6
G38	0.034 ± 0.002	20.6 ± 1.4
G45	0.031 ± 0.002	22.5 ± 1.2
U47	0.032 ± 0.001	21.7 ± 0.9
U49	0.033 ± 0.001	21.1 ± 0.8
U51	0.027 ± 0.001	25.5 ± 1.1
U75	0.027 ± 0.002	25.6 ± 1.6
U77	0.029 ± 0.002	23.8 ± 1.5
G78	0.035 ± 0.003	20.1 ± 1.5
hypoxanthine (N9-H9)	0.028 ± 0.002	24.9 ± 1.9

Table S2: Kinetic data of hypoxanthine-induced folding of the Gsw^{loop}-RNA (700MHz, 283K, [RNA]:[ligand]:[Mg^{2+}] ~1:1:8).

imino proton signal U51	k [s^{-1}]	$t_{1/2}$ [s]
1) integral 40%, all data points	0.027±0.001	25.5±1.1
2) integral 40%,*	0.029±0.002	23.8±1.7
3) integral 50%,* deconvolution	0.028±0.004	24.8±3.4
4) intensity,* variable peak position	0.029±0.005	23.9±3.8
5) intensity,* peak position constant	0.029±0.005	23.6±3.9

*time points used [s]: 0, 3.42, 7.98, 12.54, 17.1, 21.66, 26.22, 30.78, 39.9, 53.58, 71.82, 99.18, 153.9, 235.98

Table S3: Comparison of kinetic rates and time constants as obtained from different data processing methods. Imino proton signal U51 is analyzed following different procedures as indicated. Best fit is obtained for method 1) Analysis of 40% signal integral (under 2) or analysis of signal intensities (line 4 & 5) lead to almost identical kinetic values ($t_{1/2}$ [s]: 23.8, 23.9, 23.6, respectively). Analysis of signal intensity only, provides highest signal-to-noise data. Given in line 3 are the kinetic values obtained for U51 after spectral deconvolution and subsequent peak integration. The accuracy of the given kinetic parameters is not as good as our reference 1). However, the absolute value is close to the kinetic value obtained after analysis of all data points (line 1, 25.5s versus 24.8s).

References

1. Mandal, M., Boese, B., Barrick, J.E., Winkler, W.C., Breaker, R.R. (2003) Riboswitches control fundamental biochemical pathways in Bacillus subtilis and other bacteria. *Cell*, **113**, 577-86.

2. Batey, R.T., Gilbert, S.D., Montange, R.K. (2004) Structure of a natural guanine-responsive riboswitch complexed with the metabolite hypoxanthine. *Nature*, **432**, 411-5.

3. Gilbert, S.D., Reyes, F. E., Edwards, A. L., Batey, R. T. (2009) Adaptive ligand binding by the purine riboswitch in the recognition of guanine and adenine analogs. *Structure*, **17**, 857-68.

4. Buck, J., Noeske, J., Wöhnert, J., Schwalbe, H. (2010) Dissecting the influence of Mg^{2+} on 3D architecture and ligand-binding of the guanine-sensing riboswitch aptamer domain. *Nucleic Acids Res.*, **38**, 4143-53.

5. Buck, J., Fürtig, B., Noeske, J., Wöhnert, J., Schwalbe, H. (2007) Time-resolved NMR methods resolving ligand-induced RNA folding at atomic resolution. *Proc. Natl. Acad. Sci. USA*, **104**, 15699-704.